UNIVERSITY OF CALIFORNIA
RIVERSIDE

Methods for the Production of a High-Activity Positron Sources: Na-22 Coffee-Ring Minimization and Kr-79 Isotope Separation

A Dissertation submitted in partial satisfaction
of the requirements for the degree of

Doctor of Philosophy

in

Materials Science & Engineering

by

Vitaly Fedotov

March 2021

Dissertation Committee:
Dr. Allen Mills Jr., Chairperson
Dr. Elaine D. Haberer
Dr. Ward Beyermann

The Dissertation of Vitaly Fedotov is approved:

_____

_____

_____

Committee Chairperson

University of California, Riverside

ACKNOWLEDGEMENTS:

I'd like to say thank you to my professor Dr. Mills for the guidance and opportunities to learn.

Alexa Hill, thank you for being integral part in building UI and setting up the electronics for data collection in chapter 3.

Brian Lupish, thank you for helping with images and your input as a biologist.

I would also like to thank Dr. Adric Jones for brainstorming, machining, and conviviality.

ABSTRACT OF THE DISSERTATION

Methods for the Production of a High-Activity Positron Sources: Na-22 Coffee-Ring Minimization and Kr-79 Isotope Separation

by

Vitaly Fedotov

Doctor of Philosophy, Graduate Program in Materials Science & Engineering
University of California, Riverside, March 2021
Dr. Allen Mills Jr., Chairperson

Positron science can shed light into deeper understanding of materials' structures, surface electron energies, topology, porosity and other properties. To conduct this science, intense sources of positrons are required; a few source types are available, but some of them are costly and could require a lot of sophisticated apparatus. This work addresses overcoming the difficulties in the deposition of a uniform 22-NaCl isotope layer, with the goal of producing intense positron sources from radioactive isotopes at a much lower cost than currently available commercially. The first of its kind, as far as we know, apparatus for deposition of radioactive salt (22-NaCl) into a specially designed capsule is discussed in this work. This discussed design could serve as a substitute for the current 22-Na positron sources that are only available from iThemba labs in South Africa, where the deposition is done by hand pipetting the radioactive solution into the capsule designed for UHV use. Lastly, preliminary work based on isotope separation for the potential use of radioactive 79-Kr isotope as another means for intense positron source, will be discussed as well. Based on my measurements, the source designs tested in this work have shown promise to be an achievable goal. This will give labs, who are limited on funding, an

ability to afford and conduct experiments utilizing positrons, thus expanding the field of positron science and its applications to labs with different specializations. The new designs will also make possible sources of very high intensities that could be the basis for a U.S. National Positron Facility.

Table of Contents

List of Figures

Chapter 1: Introduction & Background

1.1 Introduction - History

In 1928 P. Dirac theorized the existence of an anti-electron or positron[1] as positive and negative solutions to kinetic energy levels of electrons according to quantum mechanics. In 1932 Anderson, Blackett and Occialini had obtained physical evidence of positron existence. But since Anderson published first, historically, he is credited with the discovery. In 1934 Positronium, bound state of positron-electron, was theorized by Mohorovicic Experimentally observed by Martin Deutsch in 1951.

1.2 Theory of Positron Interactions

Positron is the anti-matter particle of an electron, meaning it has exactly the same mass, $m_e = 0.9109381 \times 10^{-30}$ kg, spin of ½ just like any electron, but the charge is opposite of an electron with the value of $+1.602 \times 10^{-19}$ Coulombs (+e) instead of electron's -1.602×10^{-19} Coulombs (-e). Positronium (Ps) is the bound state of the positron (e^+) and the electron (e^-). Positronium could be considered an atom without a nucleus since both species are of the same mass, but it is a very unstable or short-lived atom. If the spins of the electron and positron are opposite and the total angular momentum of the atom is zero (↑↓ - ↓↑), then it is in a singlet state (1^1S_0), also called "para-positronium" (p-Ps) with the mean lifetime of 125 ps. When spins are parallel (↑↑, ↓↓, or an even superposition of both), however, it is then a triplet state (1^3S_1) or ortho-positronium (o-Ps) with a much longer mean lifetime of 142 ns. The binding energy for this atom is E_B= 6.803 eV. In many experiments because of such simple system, absence of protons and neutrons as a nucleus,

the only forces that need to be considered are electromagnetic forces, spin-spin interactions and recoil effects, since atom is made up of two particles with equal masses. This allows experiments to be well described by theory and therefore have less need for various correction factors, which makes modeling easier when it comes to data analysis.

Two main methods are utilized in collection of positrons: "pair production" in a particle accelerator or radioactive isotope "beta plus decay". The pair production via Bremsstrahlung or "braking radiation" from German, is possible when a charged particle loses its kinetic energy via electromagnetic interaction with another charged particle. The kinetic energy lost has to be greater than the rest mass of electron and positron, ~1.2 MeV. For example, Japanese KEK B factory slams 1-10 GeV electrons into heavy metal target, for best positron yield, a single crystal Tungsten. To increase positron production indefinitely is impossible due to heat load on the material, so the incident electron intensity or energy are optimized. From this step, slower positrons are selected and further slowed down for experiments[2]. For the labs that do not have the access to apparatus able to accelerate electrons to GeV energies, radioactive isotope method becomes a solution. Radioactive isotopes such as ^{22}Na, ^{48}V, ^{64}Cu, ^{79}Kr and many more go through beta plus (β^+) decay, converting a proton into a neutron, a positron and an electron neutrino:

$$p \rightarrow \mathrm{n} + \mathrm{e}^+ + \nu_\mathrm{e}$$

Depending on the half-life of the isotope, a different method for positron collection must be utilized. For example, in the case of ^{68}Ga, with half-life of 67.7 minutes, the isotope is made in situ from the beta decay of Ge-68 which has a 288d half-life, while ^{22}Na isotope could be made on the opposite side of the world and mounted into beamline even months

later, because half-life is much longer, 2.6 years. This work will deal with 2 isotopes: ^{22}Na and ^{79}Kr.

The first isotope that will be discussed, ^{22}Na, is currently used in Dr. Mills' lab and a specialized beamline was built around it. This isotope has properties that make it a desirable isotope to work with. First, having a half-life of 2.6 years, allows experimentalists a timeline to build and change positron beamline with some forgiveness to brightness of the positron beam. So, if your experimental set up is not completed within a month or two, the positron intensity isn't going to drop dramatically. This allows lower budget labs to have some flexibility with the available resources. Second, currently, the isotope is made in South African lab and has to travel many miles as well as spend a lot of time clearing paperwork, given the radioactivity nature. So, having a longer-lived isotope allows for a higher positron intensity by the time the isotope arrives and is mounted into the beamline. Third, since the radioactive decay of an isotope is not 100% a beta plus decay, an isotope that goes through as much of beta plus decay as possible, will therefore yield the most useful radiation. In the case of ^{22}Na, 89.8% of the radioactive decays are luckily the desired type, giving it another advantage over other isotopes. This isotope could come in a chemical compound of Sodium Chloride (^{22}NaCl) or Sodium Carbonate ($^{22}Na_2CO_3$). South African iThemba labs, currently, provide it as a Sodium Carbonate with a price tag upwards of $50'000 USD at 50 mCi activity.

Second isotope that this work will be concentrating on is ^{79}Kr. This isotope is currently only in development stages of being used in experiments. ^{79}Kr isotope yields 600-keV energy positron in 6.7% of its decays[3]. Which makes it somewhat unappealing, but

combined with the fact that half-life is 35 hours, there will be a lot more half-life decays per unit time than the ^{22}Na, so the slow positron rate would still be comparable to the ^{22}Na source. In other words, through the sheer number of decompositions with such short half-life, the positron yields would be comparable. Compared to ^{125}Xe, ^{79}Kr also has much less electrons per atom, which increases the β^+ escape depth or the thickness of the material that positrons can diffuse through, without annihilating with the surrounding electrons. With these factors, it is possible to achieve 10^{11} e^+ per second (equivalent to 3 Ci of positron activity) [3], which is far more than is produced by the current 50 mCi ^{22}Na source used at UCR Positron lab.

1.3 Positron experiments overview

To conduct a lot of experiments with positrons, a lab will need to have a source of anti-matter particles with low energies or "slow" positrons. There are many possible experiments possible, some of which will be described briefly in order for the reader to understand the importance of the research in this dissertation. Positron experiments that could be used to shed light on the nature of the world are Angular Correlation of Annihilation Radiation (ACAR), Positron Lifetime measurements, Positron-induced Auger-Electron Spectroscopy (PAES), positron channeling and Low-Energy Positron Diffraction (LEPD).

Positron channeling experiments could measure the fraction of positron penetration through the crystal lattice of a solid depending on the incidence angle of the positron beam in relation to the crystal lattice. This is a phenomenon due to the strong variation in

scattering and penetration of the beam since the particles are steered by the atomic potentials of the crystal lattice. This in turn translates into charged particle beam being channeled along the planes or axes of the solid, shown in figure below[4].

This phenomenon could be utilized in order to analyze metals or semiconductors for interstitial impurities. Since changed ions are too heavy and destructive, positrons being a non-destructive way to probe the materials will become a useful solution.

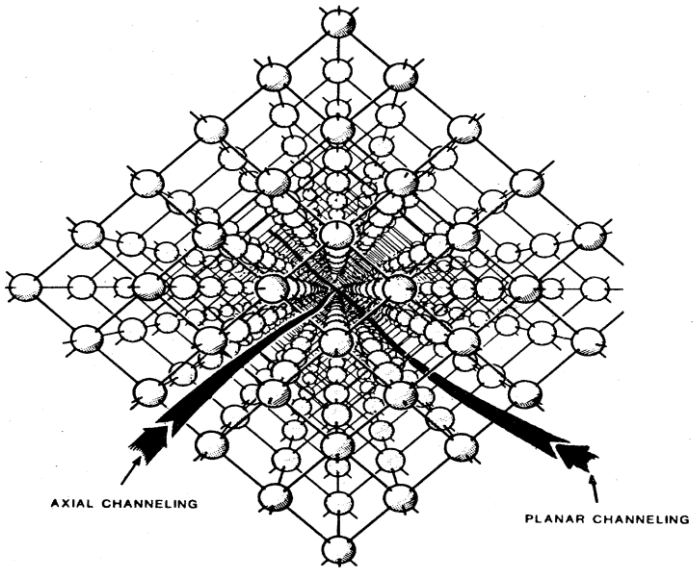

Figure 1.1 Schematic illustration of axial and planar channeling of energetic particles. The potentials that steer the incident beam are usually modeled by a continuum approximation, using cylindrically symmetric string potentials for axial channeling and two-dimensional planar potentials for planar channeling. Reproduced from reference [4]

Reemitted positron energy-loss spectroscopy (REPELS) could be a technique used to analyze vibrational modes on the surface interface[5]. For example, Fischer (1984, 1986) demonstrated the technique by observing the carbon/oxygen and carbon/nickel vibrational

modes for CO on a Ni (100) surface[6], [7]. As seen in further studies, lowering temperature, increases the resolution because of lowering the thermal spreading of positrons. Using positrons instead of electrons (Electron energy-loss spectroscopy EELS) has its advantages in the ability to probe very small energy losses (<<1 eV) compared to electrons and optics in an EELS spectrometer, as well as the absence of exchange effects, which may prove important for studies of adsorbed paramagnetic molecules[4].

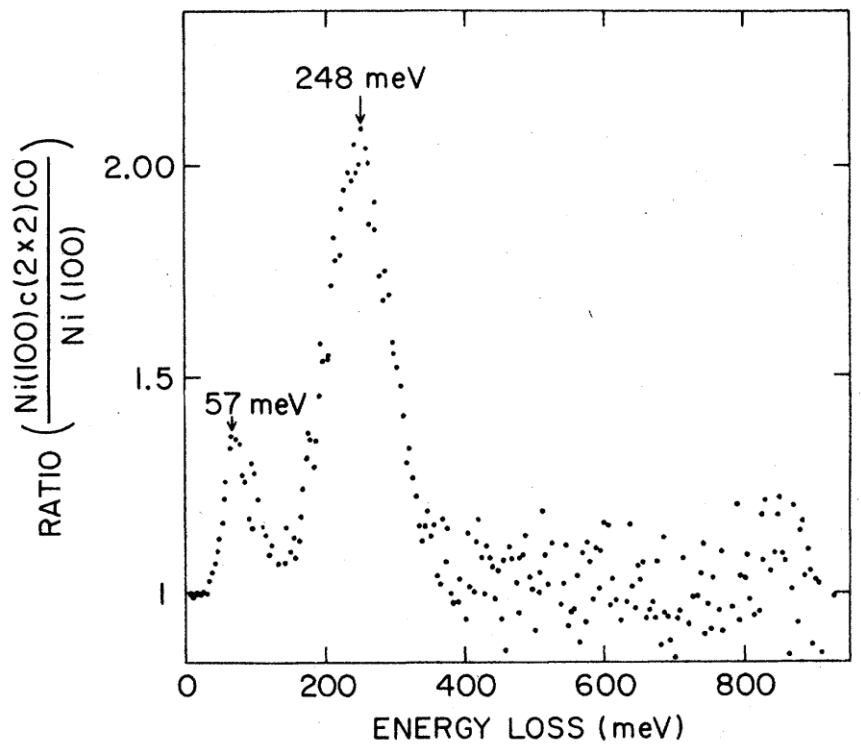

Figure 1.2 REPELS (Reemitted positron energy-loss spectroscopy) spectrum for CO on Ni(100)c(2×2)CO to clean Ni(100), showing the loss peaks for the Ni-C stretch (57 meV) and the C-O stretch (248 meV). Reproduced from reference [5]

Another type of experiment, utilizing a polarized beam of positrons or a beam where positron spins are likely to be aligned in one direction, instead of randomly, could be done in order to study surface magnetism. Since Positrons will only form triplet o-Ps (m_s =+1) with electrons if the spins are aligned, and will form both p-Ps and o-Ps (m_s =0) with equal probability if they are anti-aligned. The resulting ratio, which is normally 3:1 for a random arrangement of electrons, can be significantly affected by a preferential alignment of the spins of the electrons at the surface.

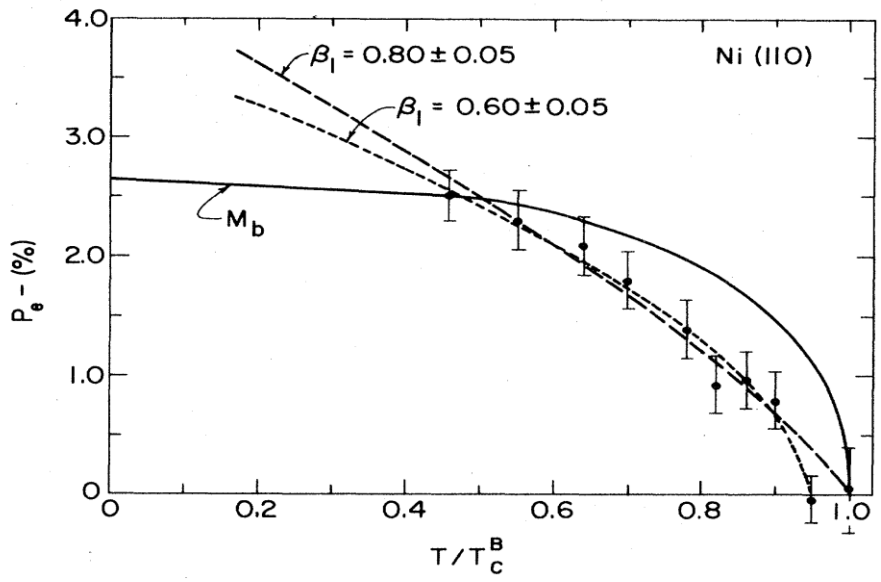

Figure 1.3 Temperature dependence of the spin polarization P_e of the electron captured at a Ni(110) surface to form Ps. The solid curve is based on the bulk magnetization properties of Ni (normalized to the lowest-temperature data), and the dashed and dotted curves are models for surface magnetization with the critical temperature $T_c=T_c^B$ and T_c unconstrained, respectively. Reproduced from reference [8]

Positrons trapped at surface of a material could become trapped or localized at the surface and annihilate there. These annihilations could produce Auger electron emission [9] and therefore be a sensitive probe for surface impurities or defects in a material. This type of information could be used to analyze usefulness of techniques used to make the material in respect to defects associated with those techniques. This could be very useful, but not limited to semiconductor industry.

Positron interactions with matter are an important to study because it could become a very useful tool in broadening our understanding of this universe just like a microscope or an electron microscope did. Defect profiling could be done in multiple applications of materials science, such as bilayer and multi-layer systems. This could be especially useful when it comes to studying wear, corrosion and analyzing new growth techniques for novel materials or epitaxial multilayer systems.

1.4 References

[1] P. A. M. Dirac, “The quantum theory of electron,” vol. 43, no. 1927, pp. 610–624, 1937.

[2] T. Suwada *et al.*, “First application of a tungsten single-crystal positron source at the KEK B factory,” *Phys. Rev. Spec. Top. - Accel. Beams*, vol. 10, no. 7, pp. 1–6, 2007, doi: 10.1103/PhysRevSTAB.10.073501.

[3] A. P. Mills, Jr. “Suitability of Kr-79 as a Reactor-Based Source of Slow Positrons,” *Nucl Sci Eng.*, no. 110, pp. 165–167, 1990.

[4] P. J. Schultz and K. G. Lynn, “Interaction of positron beams with surfaces, thin films, and interfaces,” *Rev. Mod. Phys.*, vol. 60, no. 3, pp. 701–779, 1988, doi: 10.1103/RevModPhys.60.701.

[5] D. A. Fischer, K. G. Lynn, and W. E. Frieze, “Reemitted-positron energy-loss spectroscopy: A novel probe of adsorbate vibrational levels,” *Phys. Rev. Lett.*, vol. 50, no. 15, pp. 1149–1152, 1983, doi: 10.1103/PhysRevLett.50.1149.

[6] D. A. Fisher, “Ph. D. dissertation.” Available from University Microfilms International (No.85-13537), New York State University, Stony Brook, 1984.

[7] D. A. Fischer, K. G. Lynn, and D. W. Gidley, “High-resolution angle-resolved positron reemission spectra from metal surfaces,” *Phys. Rev. B*, vol. 33, no. 7, pp. 4479–4492, 1986, doi: 10.1103/PhysRevB.33.4479.

[8] D.W. Gidley, “Polarized Low-Energy Positrons: A New Probe of Surface,” *Phys. Rev. Lett.*, vol. 49, no. 24, pp. 1779–1783, 1982.

[9] WEISS A, MAYER R, JIBALY M, LEI C, MEHL D, LYNN KG, “Auger-Electron Emission Resulting from the Annihilation of Core Electrons with Low-Energy Positrons”, *Phys. Rev. Lett*. 61, 2245 - 2248 (1988).

Chapter 2: Coffee-ring minimization for the production of high-activity ^{22}Na positron sources

2.1 Introduction

We describe a method to deposit a uniform layer of NaCl from an aqueous solution for the purpose of fabricating high activity sources of ^{22}Na for experiments using positrons. For minimum attenuation of the emitted positrons, it is desirable to produce a NaCl deposit on a flat substrate without the formation of either large isolated crystals or a thick salt deposit or "coffee ring" around the edge of the evaporating drop. We have eliminated these effects using a computer-controlled syringe, the tip of which is in close proximity to the heated substrate surface, to supply the salt solution at a constant rate. By this means a continuous drop size is maintained throughout the deposition of 10 ml of solution over the course of 10-12 hours. Dry N_2 at a temperature of 90 °C directed symmetrically at the surface of the droplet ensures rapid evaporation and the presence of steady advantageous fluid currents. The peak-to-peak variations in the resulting deposit are typically less than ±50% of the mean density.

Many positron beam systems today use a solid rare gas[1] moderator [2] to obtain a ~1% yield of "slow" (1-2 eV) positrons from the beta-decay positrons of a radioactive ^{22}Na source [3]. The slow positrons are accelerated to form beams of positrons with a variety of characteristics suitable for measurements of the properties of solids, surfaces, and atomic systems. Sealed sources of ^{22}Na with a maximum source activity of ~50 mCi

are presently available from iThemba labs [4] in South Africa. In this paper we outline a method for depositing uniform layers of ^{22}NaCl on a substrate, with the goal of producing sealed sources with target activities of ~100 mCi or higher [5] with minimal loss of the effective source strength due to the absorption of beta particles associated with nonuniform crystallization of the salt deposit.

In deposition of a precipitate from solution it is not uncommon to observe the formation of a ring stain or "coffee ring" [6], a circular deposit reminiscent of that left by the bottom of a coffee cup on a tablecloth. Coffee ring morphology has been shown to be dependent on salt concentration and substrate temperature [7], [8]**.** This coffee ring formation is a problem in a variety of fields, such as, ink printing, gene mapping and characterization, as well as the deposition of probes onto the surface of microarrays for DNA/RNA research [9]. For our purposes, thicker coffee ring of ^{22}NaCl would mean higher absorption of positrons by the salt deposit, but another issue would be secondary electron production. That is because energetic positrons slow down within the salt deposit via ionization[10]. Ejected secondary electrons could have large energy spread and become a background noise issue.

A handful of strategies have been developed to mitigate this effect, but they're not universally applicable. It has been shown that if the shape of the molecules to be deposited is changed to long rods [11], [12] or if cellulose nanofibers are mixed into the solution [13], then the capillary flow inside the drop is altered, and the resulting deposition is significantly

more uniform. Another method to achieve a uniform deposit, is to produce a spontaneous electric field within the droplet by choosing salts for which the diffusivity of either the cation or anion is higher to make changes in the electrokinetic transport of the particles and of the fluid near the substrate surface [14]. For our purposes, it is undesirable to attach the ^{22}Na atoms to long molecules or add other impurities, as this will result in a higher absorption coefficient owing to the larger mass deposited per activity. As such we have found an alternative means of preventing coffee ring formation through controlling the environment in which the deposition and drying occurs in.

Due to the risk of radioactive contamination within a hot cell during deposition of radioactive material, and particularly considering the volume of solution that needs to be evaporated, it is undesirable to have drops falling from the deposition syringe or multiple drops breaking free of the syringe tip after the drop makes contact with the deposition surface. This is because when a drop formed at the end of a syringe breaks free, it can become electrostatically charged [15] and produce smaller secondary charged droplets that can be carried away by airflow and stray electric fields. Microscopic drop formation between the primary drop and the syringe can thus result in dispersion of stray activity within the hot cell due to repulsive electrical forces and the force of the N_2 gas flow. To circumvent this problem our deposition involves a continuous meniscal contact between the syringe and deposited drop. By carefully moderating the flow of solution from the syringe we thus have a stable deposition, with no change in drop volume during the production of a source of desired activity.

In experiments on depositing NaCl solutions, we have noticed that as the evaporation rate is decreased, the coffee ring is correspondingly thicker. Thus, to minimize the coffee ring effect, we must increase the evaporation rate by heating the substrate. To counteract the capillary flow associated with this process we also find it necessary to flow heated dry N_2 gas over the drop during deposition to develop beneficial Marangoni Flow [16]. This approach results in an increased evaporation rate without developing turbulent drop activity.

2.2 ^{22}Na sources

The theoretical maximum specific activity of ^{22}NaCl is 2.39 kCi/g while $^{22}Na_2CO_3$ is slightly higher, 2.64 kCi/g for comparison. The narrow beam exponential attenuation rate of ^{22}Na betas is λ = 35 cm^2/g [17]. Fig. 2 shows the fraction t of the positrons transmitted through a foil of dimensionless thickness λd (here d is the foil thickness in units of mass per unit area, g/cm^2) given a thin radioactive source in contact with the back of the foil. Here, t is approximated assuming the beta intensity is attenuated exponentially and neglecting scattering, which results in the expression

$$t = \int_0^1 \exp\{-\lambda d / z\} dz$$

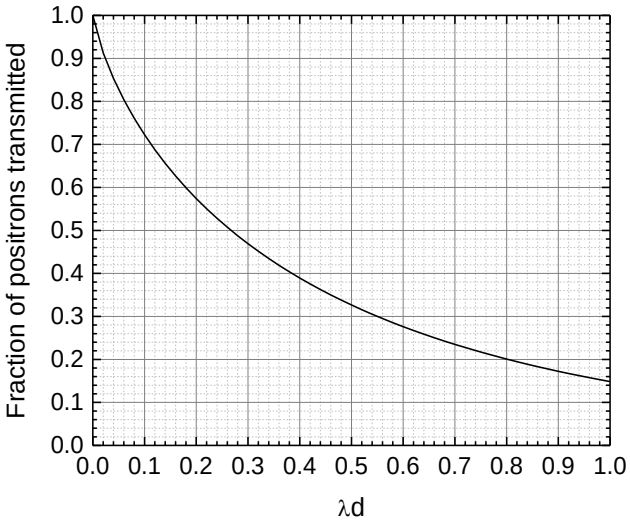

Figure 2.1 Transmission probability of ^{22}Na betas from a point source through a layer of dimensionless thickness λd. The source is in contact with the back of the layer.

We may approximately correct for a source of non-negligible thickness by increasing the effective foil thickness by half the source thickness. A sheet of activity of dimensionless thickness $\lambda d = 0.2$ plus a 5 μm Ti window for which $\lambda d = 0.08$ gives a total mean thickness $\lambda d = 0.18$ and about 60% transmission of the betas. Thus, the Na content per unit area for a practical source is $d \approx 0.2/\lambda = 5.7$ mg/cm^2 = 6.5×10^{19} ^{22}Na atoms/cm^2. The decay rate per unit area is 6.5×10^{19} ^{22}Na atoms/cm^2 / 1.18×10^{8} s = 5.5×10^{11} decays/cm^{2}s = 14.9 Ci/cm^2. An ideal 6 mm diameter source of area 0.29 cm^2 would thus have an activity of 4.3 Ci. Roughly half the Na might be ^{23}Na if the isotopes are made by spallation from Mg or Al targets so the maximum activity would be 2.15 Ci for this source area. With the quoted specific activity of 0.8 kCi/g which is about 1/3 of the

theoretical maximum, it should be possible to make 6 mm diameter ^{22}Na sources with 500 mCi total activity and 60% beta efficiency. Since the decay products, Ne, CO, CO_2 and O_2 may be partly removed over time, the source efficiency may improve somewhat with age.

A positron source comprises a radioactive salt deposited in a capsule with a titanium foil window 5 μm thick. The beta decay of ^{22}Na to ^{22}Ne produces a 1.274 MeV nuclear gamma ray along with a 560 keV endpoint energy positron in 90% of the decays. The production of useful high activity sources introduces a new potential issue, the buildup of Ne gas in the sealed capsule which could possibly burst the window foil. To solve this potential problem, and to permit the use of much larger area thin windows, our source capsule design incorporates a tunable micro-leak to vent the Ne gas. Thus, we should be able to accommodate 4 times higher activity sources by increasing the surface area of the deposition substrate by a factor of ~4.

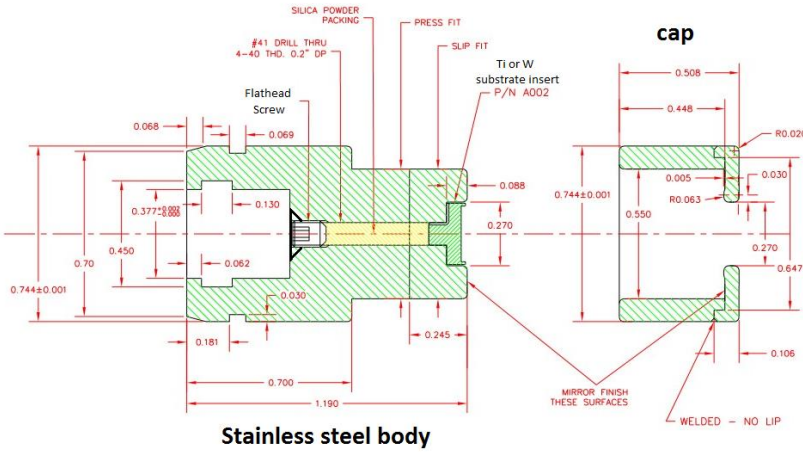

Figure 2.2 Machine drawing of the source capsule.

Figure 2.3 Source capsule. (Stainless steel body)

A 100 mCi source will require a minimum of 42.6 μg of NaCl (7.29×10^{-7} moles). Solutions with an activity of up to 17 mCi/mL are available from Los Alamos National Lab (LANL), thus requiring the deposition of 5.88 mL (minimum 1.24×10^{-4} M) of solution for a 100 mCi source. To produce an accurate solution of comparable concentration, we first prepared a concentrated 22NaCl solution of 0.23766 M. This was then diluted by mixing 5.9 μL into 10 mL of deionized water, yielding a 1.40×10^{-4} M solution.

2.3 Description of source capsule

The source capsule, depicted in the drawing of Fig. 2, is constructed primarily of 304 stainless steel. The body cylinder is ~19 mm in diameter and houses a titanium inset

with a ~7 mm diameter that serves as the substrate for deposition. The inside diameter of the titanium substrate is approximately 6 mm. Assuming a 5 mm diameter deposition (as seen in Fig. 3), the total volume deposited to yield 100 mCi is 1.929 mm^3, *i.e.*, a uniform layer 98 μm thick. Through the center of the capsule a tapped hole contains a flat-head screw to produce a controlled leak of the desired size, which provides a mechanism to vent the Ne produced by the radioactive decay of ^{22}Na. For a source of order 1 Ci, the accumulation of Ne over a period of ~1 year would approach 0.1 atm without venting, a pressure differential that could compromise the foil seal. This is not anticipated to be a major issue, but the design is there for extra safety. The 5 μm Ti cover foil is prepared by loosely binding it to the capsule lid via a thin layer of high-vacuum grease. The permanent seal is made by carefully tightening the screws holding the lid onto the capsule. A semi-circular raised ring, similar to that used in VCR gas connectors, provides the sealing surface, with the foil pressed between the flat surface of the capsule and the raised ring. A locating pin guides the lid into place and ensures the correct alignment during installation. The six screws used to attach the lid are installed via a computer-controlled torque wrench. The foil seals the radioactive material, preventing contamination in transport or during use in a positron beam apparatus.

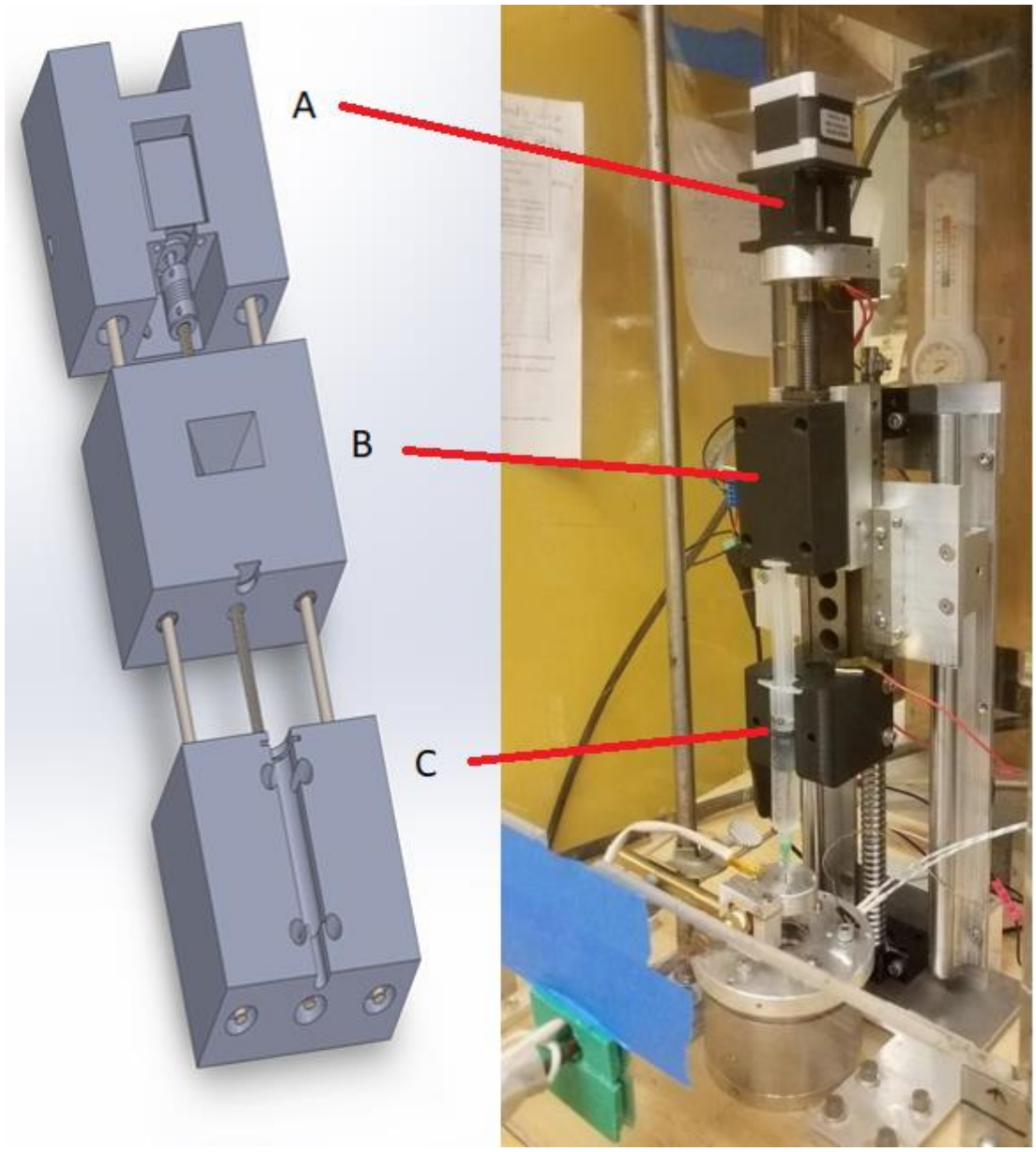

Figure 2.4 Deposition system. A) motor mount B) plunger control C) Syringe holder

2.4 Source preparation

The controlled deposition must be achieved via an automated or remotely controlled procedure to minimize exposure to the personnel involved. The test rig involves a syringe mounted above the target substrate. The assembly is controlled via an Arduino

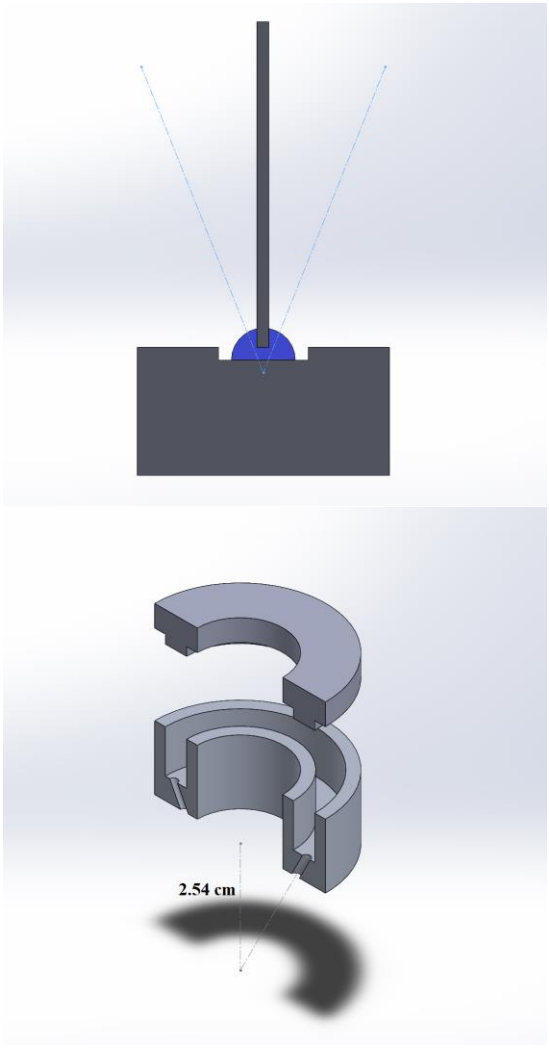

Figure 2.5 Detail of gas flow distributor (bottom image). Model of N_2 gas flow (dashed lines) over drying drop (top image)

Uno, with a ball screw drive attached to the syringe plunger, driven via a stepper motor. The stepper motor, a NEMA 18 model, has a default of 400 steps per turn (which can be further increased using micro-stepping), which drives a 1 mm pitch threaded rod. The

deposition of 10 mL may be accomplished using a deposition time of 10-12 hours which would be optimal for a delivery rate of 0.5-0.9 µL of solution per minute. The tip of the syringe is mounted through a custom gas distributor, which controls both the spread and flow rate of gas over the droplet. The gas flow distributor (Fig. 5) is a small annulus, connected via a single inlet which delivers heated dry N_2, and distributes the gas via 8 small (~1mm or 0.040in diameter) holes, which are arrayed in a circle and are angled toward the droplet, aligned to a central focus, 25 mm below the distributor. The source substrate is positioned such that the gas does not reach a focus, but instead evenly covers the entire droplet, allowing for rapid and uniform evaporation.

The technique of flowing dry N_2 does not solely aid in evaporation, but also affects the shape of the drop by altering the dynamics of the capillary flow within the droplet which strengthens the Marangoni flow [6, 16]. The force of the gas flowing over the drop causes it to flatten, which aids in uniform deposition by increasing the ratio of the surface area to volume. In our understanding, the lower ratio also leads to less capillary flow, which is a natural result of the evaporation process. In the experiments to date, the ideal conditions involve flowing N_2 heated to ~90^{o}C (though the effective temperature at the substrate may be somewhat lower), flowed at a rate of 3-7 L/min. The maximum temperature of the gas must be kept well below the boiling point of water in order to avoid the risk of bubbling within the droplet, which could potentially lead to sputtering of radioactive material within the hot cell.

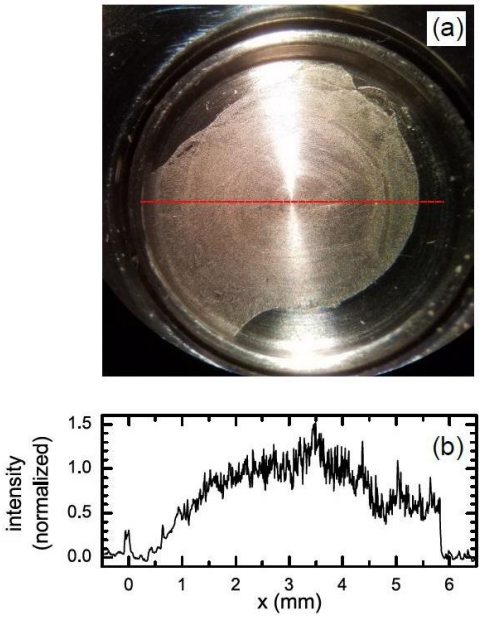

Figure 2.6 a) Image of salt deposit and b) Reflected light intensity along the line indicated.

Our most successful deposition was made using a 90°C N_2 flow of 7 L/min, with the focal point of the gas flow 2.5 mm below the surface of the substrate. The substrate temperature was 75°C and the end of the syringe needle was 1 mm from the bottom of the substrate, to minimize the solution's adhesion to the needle. The result of this deposition, illustrated in Fig. 6a was a lopsided but quite uniform deposit. In Fig. 6b the intensity of a slice through the center of the deposition provides a measure of the layer uniformity**.** The mean and the standard deviation from the mean over the range 0.4-5.9 mm along the line indicated in Fig. 2.6b is approximately 0.75±0.25.

Figure 2.7 shows a couple of failed experiments in which various parameters were being optimized. Top left (a) is the result of having the drop evaporate too slowly, therefore a much thicker coffee ring border. Reason for slower evaporation were the settings for 5 LPM of gas flow at 82 ^{o}C. Even though, the temperature of the gas flow was higher than the successful run, the amount of gas flow was lower, decreasing the evaporation rate compared. Next two examples (b and c) are of similar settings with gas temperature fluctuations between 70 ^{o}C-78 ^{o}C. As for the bottom right image (d), the drop size was not constant due to various technical issues and therefore the multiple coffee ring pattern was the result.

a) 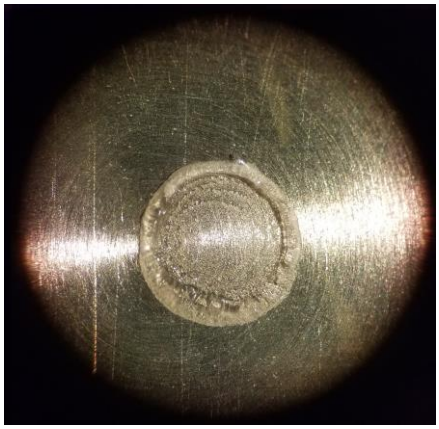

b) 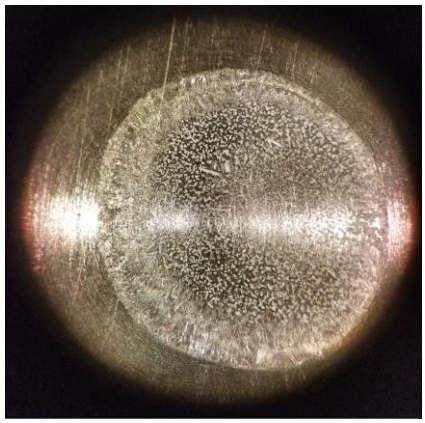

c) 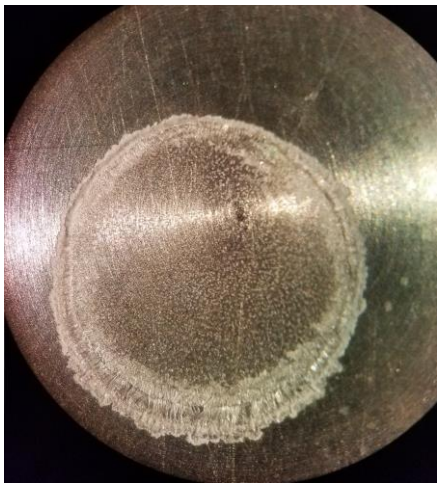

d) 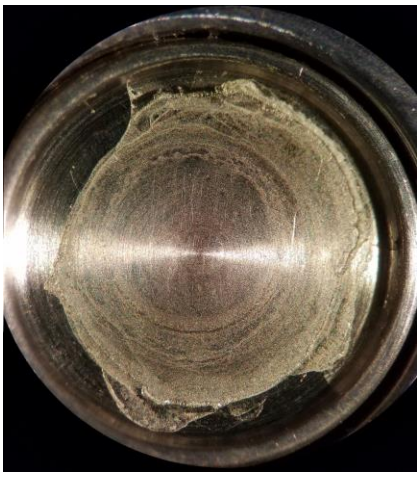

Figure 2.7 examples of failed experiments. a) result of a slow evaporation b) & c) results of varied gas temperature during the evaporation process d) result of a varied drop size during the evaporation

2.5 Concluding Remarks

Our particular approach provides a technique for relatively uniform deposition which does not require adulteration of the deposited solution. For methods relying on the purity of the deposit, our method becomes valuable. Using our apparatus and deposition technique, we have achieved a uniform layer of NaCl deposited on a titanium substrate. Titanium was chosen as a substrate because of the low atomic number, which helps to maintain the polarization of the positron beam by reducing the fraction of positrons that are backscattered [18]. While higher fast-positron-to-slow positron efficiencies can likely be achieved with a tungsten substrate, the reflected positrons tend to be spin flipped, leading to a reduction in net polarization. This could be critical in future efforts to produce a Ps BEC [19, 20] where spin quenching would result in a reduction of the achievable Ps density. In future experiments of this type one could explore the impact of substrate surface treatments on the uniformity of deposition, and study the rate of deposition and dynamics of the salinity within the needle / drop system. Preliminary tests with small radioactive samples will allow testing for contamination in the deposition process.

2.6 References

[1] A. P. Mills and E. M. Gullikson, "Solid neon moderator for producing slow positrons," *Appl. Phys. Lett.*, vol. 49, no. 17, pp. 1121–1123, 1986, doi: 10.1063/1.97441.

[2] K. F. Canter, P. G. Coleman, T. C. Griffith, and G. R. Heyland, "Measurement of total cross sections for low energy positron-helium collisions. (Positron backscattering from metal surface)," *J. Phys. B At. Mol. Phys.*, vol. 5, no. 8, 1972, doi: 10.1088/0022-3700/5/8/007.

[3] T. D. Steiger, J. Stehr, H. C. Griffin, J. H. Rogers, M. Skalsey, and J. Van House, "Development of intense, long-lived positron sources," *Nucl. Inst. Methods Phys. Res. A*, vol. 299, no. 1–3, pp. 255–260, 1990, doi: 10.1016/0168-9002(90)90787-7.

[4] C. Naidoo, N. P. van der Meulen, C. Vermeulen, and R. Krause-Rehberg, "THE PRODUCTION OF 22Na POSITRON SOURCES AT iTHEMBA LABS," *Abstr. ICPA-16*, p. 22, 2013.

[5] H. Huomo *et al.*, "Deposition and characterization of 22Na sources for use with monoenergetic positron beams," *Nucl. Inst. Methods Phys. Res. A*, vol. 284, no. 2–3, pp. 359–364, 1989, doi: 10.1016/0168-9002(89)90302-1.

[6] R. D. Deegan, O. Bakajin, T. F. Dupont, G. Huber, S. R. Nagel, and T. A. Witten, "Capillary flow as the cause of ring stains from dried liquid drops," *Nature*, vol. 389, no. 6653, pp. 827–829, 1997, doi: 10.1038/39827.

[7] N. Basu and R. Mukherjee, "Evaporative Drying of Sodium Chloride Solution Droplet on a Thermally Controlled Substrate," *J. Phys. Chem. B*, vol. 124, no. 7, pp. 1266–1274, 2020, doi: 10.1021/acs.jpcb.9b08809.

[8] G. Chaniel, M. Frenkel, V. Multanen, and E. Bormashenko, "Paradoxical coffee-stain effect driven by the Marangoni flow observed on oil-infused surfaces," *Colloids Surfaces A Physicochem. Eng. Asp.*, vol. 522, pp. 355–360, 2017, doi: 10.1016/j.colsurfa.2017.03.009.

[9] M. C. Pirrung, "How to make a DNA chip," *Angew. Chemie - Int. Ed.*, vol. 41, no. 8, pp. 1276–1289, 2002, doi: 10.1002/1521-3773(20020415)41:81276::AID-ANIE12763.0.CO;2-2.

[10] M. Eldrup, A. Vehanen, P. J. Schultz, and K. G. Lynn, "Positronium Formation and Diffusion in a Molecular Solid Studied with Variable- Energy Positrons,"

Phys. Rev. Lett., vol. 51, no. 21, pp. 2007–2010, 1983, doi: 10.1017/CBO9781107415324.004.

[11] V. R. Dugyala and M. G. Basavaraj, “Evaporation of sessile drops containing colloidal rods: Coffee-ring and order-disorder transition,” *J. Phys. Chem. B*, vol. 119, no. 9, pp. 3860–3867, 2015, doi: 10.1021/jp511611v.

[12] H. H. Sun *et al.*, “Evaporation of saline colloidal droplet and deposition pattern,” *Chinese Phys. B*, vol. 29, no. 1, 2020, doi: 10.1088/1674-1056/ab5782.

[13] Y. Ooi, I. Hanasaki, D. Mizumura, and Y. Matsuda, “Suppressing the coffee-ring effect of colloidal droplets by dispersed cellulose nanofibers,” *Sci. Technol. Adv. Mater.*, vol. 18, no. 1, pp. 316–324, 2017, doi: 10.1080/14686996.2017.1314776.

[14] R. Guha, F. Mohajerani, A. Mukhopadhyay, M. D. Collins, A. Sen, and D. Velegol, “Modulation of Spatiotemporal Particle Patterning in Evaporating Droplets: Applications to Diagnostics and Materials Science,” *ACS Appl. Mater. Interfaces*, vol. 9, no. 49, pp. 43352–43362, 2017, doi: 10.1021/acsami.7b13675.

[15] D. Choi *et al.*, “Spontaneous electrical charging of droplets by conventional pipetting,” *Sci. Rep.*, vol. 3, pp. 1–7, 2013, doi: 10.1038/srep02037.

[16] H. Hu and R. G. Larson, “Marangoni effect reverses coffee-ring depositions,” *J. Phys. Chem. B*, vol. 110, no. 14, pp. 7090–7094, 2006, doi: 10.1021/jp0609232.

[17] R. D. Evans, “Nuclear Effects of Nuclear Moments,” *The Atomic Nucleus*. McGraw Hill, NY 1955, p. 627-629; M. Curie, A. Debierne, A. S. Eve, H. Geiger, O. Hahn, S. C. Lind, St. Meyer, E. Rutherford, and E. Schweidler, "The Radioactive Constants as of 1930 Report of the International Radium-Standards Commission", *Rev. Mod. Phys.* **3**, 427 (1931).

[18] A. Rich, R. S. Conti, D. W. Gidley, and M. Skalsey, “Production and applications of monoenergetic polarized positron beams,” *Hyperfine Interact.*, vol. 44, pp. 125–137, 1988.

[19] E. P. Liang and C. D. Dermer, “Laser cooling of positronium,” *Opt. Commun.*, vol. 65, no. 6, pp. 419–424, 1988, doi: 10.1016/0030-4018(88)90116-2.

[20] P. M. Platzman, “Surface positrons and the many positron, many electron system”, in Positron Studies of Solids, Surfaces, and Atoms, A.P. Mills Jr., W. S. Crane, and K. F. Canter, eds. (World Scientific, Singapore, 1986) pp. 84-101.

Chapter 3: Krypton Isotope Separation

3.1 Introduction

The idea of isotopes, “elements may have two or more forms with distinguishable atomic masses, but indistinguishable chemically”, has been formed in 1913 by Frederick Soddy [1]. Soddy confirmed this conclusion and published a paper on average atomic mass of stable Lead from ores rich in Uranium (206.08) and ores rich in Thorium (207.69), since these ores decay into different isotopes of Lead. Having the same number of protons, making it Lead, but a different number of neutrons, making one isotope of Lead heavier than the other. Shortly after, using a primitive spectrograph, J.J. Thomson discovered presence of Metaneon (Neon-22) in known atmospheric Neon-20 that was known at that time. Device subjected positively charged ions of gaseous atoms to a magnetic field, bending the path of lighter atoms more than that of the heavier ones. Thomson’s assistant, Francis W. Aston, went on to develop a much more powerful device “Mass Spectrograph” and in 1922 was awarded a Nobel Prize in Chemistry. By 1935, most isotopes and their relative abundances were known.

The understanding and use of isotopes were the key to nuclear weapons and nuclear power plants. Today, isotopes are a part of everyday life in the form of a common household smoke detector. In the medical field, radioisotopes are utilized in nuclear medicine anywhere from detection to destruction of cancer cells to analyzing blood flow to organs, to assessing bone growth as well as functioning of the organs. In creation and separation of various isotopes, many life’s problems could become a thing of the past. Nuclear weapons and power plants require a large supply of enriched nuclear fuel and

that is a very expensive endeavor. Many breakthroughs were made in order to make this less costly and more efficient, one of them was Zippe-type centrifuges in 1950s, which is based on mass difference separation that will be discussed later. Isotopes of Krypton could be a valuable asset to any positron research lab. Development of a new technique that is cheaper and scalable is the subject of this chapter.

3.2 Theory

Isotope separation techniques have two main principles on which they operate: mass difference or chemical reaction rates of isotopes. Basics of diffusion, centrifuge and electromagnetic methods will be lightly touched upon for the purpose of general information, since each method could have a separate book written about it. There are many more methods for isotope separation, with major ones being kept under government secrecy.

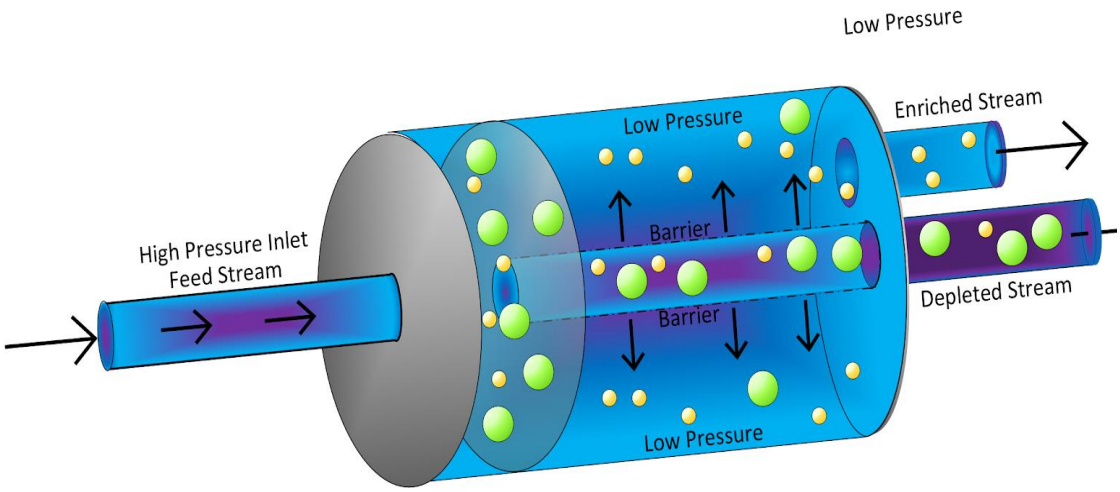

Figure 3.1 Gas diffusion method relies on lighter isotope diffusion being higher than that of heavier isotopes.

3.2.1 Diffusion Method

Gas diffusion is based on the principle of the lighter atoms or molecules being able to diffuse from an area of higher concentration to an area of lower concentration at a faster rate than heavier atoms or molecules. Graham's Law describes the process:

$$\frac{\text{Rate}_\text{L}}{\text{Rate}_H} = \sqrt{\frac{\rho_\text{H}}{\rho_L}}$$

Where Rate_L and Rate_H refer to the diffusion rate of "light" and "heavy" atoms or molecules and ρ_H and ρ_L refer to density of "light" and "heavy" particles or molecules respectively[2].

Harkins was the first to separate the isotopes of Chlorine [3], [4], [5] perfected the gas diffusion column.

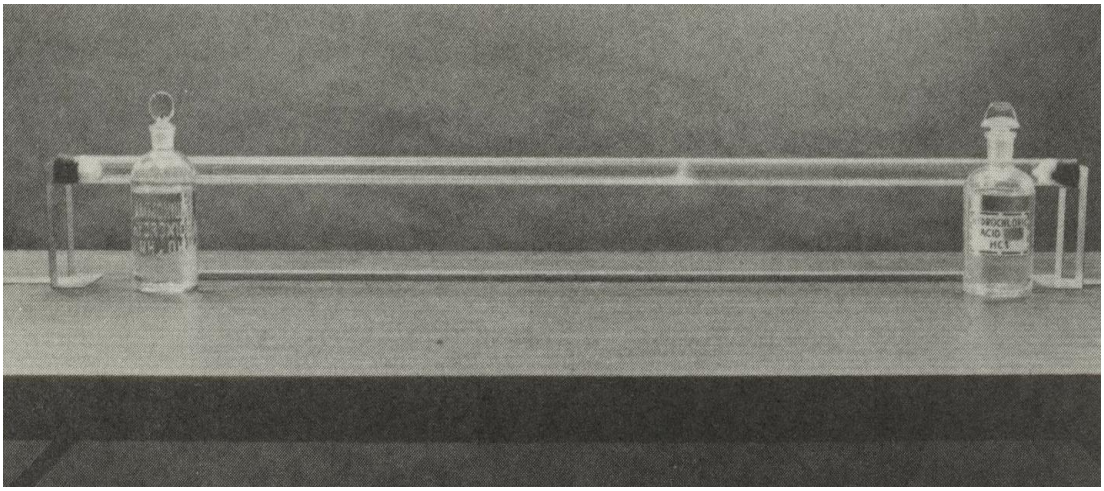

Figure 3.2 Demonstration of diffusion of gases: Cotton soaked in Ammonia ($NH_{3(g)}$ 17.03 g/mol) on left and $HCl_{(g)}$ (36.46 g/mol) on the right, placed inside a long tube. White deposit (ammonium chloride $NH_4Cl_{(s)}$) is formed where gases meet. Since $HCl_{(g)}$ is heavier, the deposit is closer to the right. Reproduced from reference [2]

Once the gas mixture is in thermal equilibrium, the "light" and "heavy" gas molecules will have the same kinetic energy (KE_L or KE_H), but different speeds (v_L and v_H referring to speed of light and heavy particles respectively), because of the momentum difference due to the difference in mass (m_L and m_H referring to mass of light and heavy particles respectively). And it could be shown through this equation:

$$KE_L = KE_H$$

$$\frac{1}{2}m_L v_L^2 = \frac{1}{2}m_H v_H^2$$

Simplifying and rearranging yields the basic principle of the diffusion isotope separation:

$$\frac{v_L}{v_H} = \sqrt{\frac{m_H}{m_L}}$$

This equation could reliably predict the amount of enrichment per stage, based on the mass difference. Since the difference in mass of U-238 and U-235 is only 3 amu (atomic mass units), the U-235 atom would travel only 0.6% faster than U-238. However, in enrichment plants, Uranium Hexafluoride is the gas that is purified, the mass difference between heavy and light molecules is even smaller, therefore lowering the speed difference between the two molecules. Such tiny mass difference is the reason for needing a large array of stages. Getting to high levels of purity through diffusion only is very energy costly. That is why other methods are preferred.

3.2.2 Centrifuge Method

This method involves the principle of heavier particles, due to centrifugal force, pushing their way towards the edges inside a spinning cylinder and lighter isotopes, therefore, accumulating in the center[6]. With this gradient of heavier to lighter isotopes along the radius of the spinning cylinder, the isotope separation is possible. This design is repeated multiple times in order to achieve higher levels of concentration for the desired isotope. One of the perks for this method is that it is a continuous process and doesn't need batching.

The difficulties with the progress of centrifuge enrichment process include, finding appropriate materials for the centrifuge as it spins at high RPM and avoidance of lingering in destructive resonance frequencies. Current technologies behind centrifuge

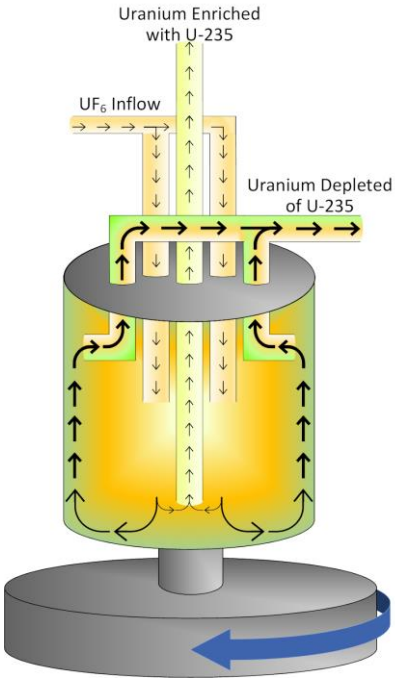

Figure 3.3 diagram of uranium enrichment via centrifuge

enrichment are kept under government secrecy. The biggest reason, behind secrecy, is to keep the possibility of nuclear weapons being widely available.

3.2.3 Electromagnetic Method

Analogous to mass spectroscopy, but with scaled up apparatus called calutron, electromagnetic method isotope separation method utilizes mass difference of each isotope. Charged gas particles are sent through a magnetic field which bends their path. Isotopes with more neutrons are heavier, while still having the same charge as the lighter isotopes. The lighter isotopes, therefore, experience more deflection than the heavier ones and the separated streams could be collected by different receivers [7].

Basic principle behind this method could be described by the following math. When charged particle enters the chamber with the magnetic field ($\vec{B}$) perpendicular to the velocity ($\vec{v}$) of the particle, the separation due to centripetal force caused by electromagnetic interactions begins.

$$\frac{mv^2}{r} = q\vec{v} \times \vec{B} = qvB$$

When the above expression is simplified for the radius of deflection (r), it becomes obvious that the larger the mass of the particle (m) with charge q, the larger the radius. In other words, the heavier isotope's path is bent less.

$$r = \frac{mv^2}{qvB} = \frac{mv}{qB}$$

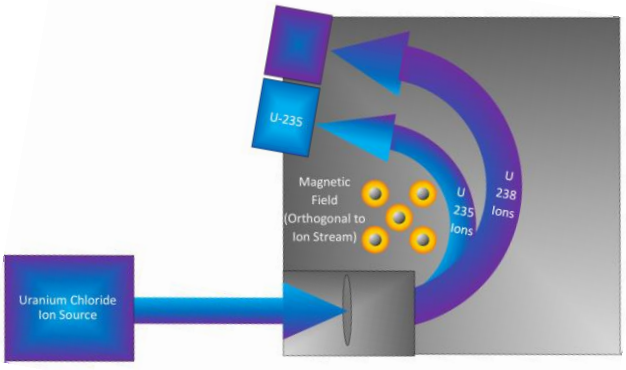

Figure 3.4 Diagram of calutron principle of operation.

U-235 trajectory radius (r) is smaller than that of the U-238 by 0.6%. At the radius of 2 feet, the difference in trajectory would be 0.3 inches. To achieve precise strength of the magnetic field, the voltage and current would have to be controlled better than 0.1%. In 1942, a single Calutron could produce 4 grams of enriched uranium per day.

By 1945, Oak Ridge, the Secret City had 75,000 people living and working there. Y-12 plant had a large number of women working there, also called “Calutron Girls”. With many young men serving overseas, demand for female labor force has increased and thousands of women were drawn to jobs at Clinton Engineer Works, which was a front for the Manhattan Project. These women were unknowingly, due to secrecy, changing the human history by supporting the development of the world’s first atomic

weapon[8]. Although feedback was invented at Bell labs by Harold Black in 1927, it was not available for stabilizing the magnet currents for the 1152 calutrons at Oak ridge. This task was left to the Calutron Girls.

For many young women, working at Clinton Engineer Works was the first time they had left their families and rural lifestyle. Although it wasn't a big city like Nashville or Memphis, Oak Ridge had movie theaters, roller rinks, recreation centers, and other places for young people to socialize and have fun. Living in dormitories and earning money was an exciting and empowering experience for many of the women living in Oak Ridge.

Figure 3.5 Ed Wescott's famous photo of "Calutron Girls" at Y-12 Plant
Reproduced from reference [5]

With Kr_{79} half-life being 35.04 hours, the decay constant could be calculated to be:

$$\lambda = \frac{0.693}{t_{\frac{1}{2}}} = 5.5 \times 10^{-6} s^{-1}$$

Using this constant to calculate the number of atoms (N_0) of Kr-79 required to make a 100 mCi ($A_0 = 3.7\times 10^9$ Becquerel or disintegrations per second) source here:

$$N_0 = \frac{A_0}{\lambda} = \frac{3.7 \times 10^9 s^{-1}}{5.5 \times 10^{-6} s^{-1}} = 6.7 \times 10^{14}$$

Using the molar mass of 77.92 for Kr-78, we find the necessary isotopic mass (M) required for a 100 mCi source:

$$M = \frac{6.7 \times 10^{14}}{6.022 \times 10^{23} mol^{-1}} \times \frac{77.92 g}{mol} = 8.7 \times 10^{-8} g$$

With the lab requirement of only 870 μg to carry out most experiments, this method is viable depending on cost and availability of the necessary equipment.

With much larger mass difference between Kr-78 (0.36% rel. abundance) and Kr-84 (57% rel. abundance), compared to U-235 and U-238, the path difference between Krypton isotopes (Kr-84/Kr-78) would be on the scale of 7.7% or 3.5 inches if parameters are similar to 1942 uranium enrichment calutron at Y-12 Plant. This would allow for more efficient separation of isotopes, when compared to $UF_{6(g)}$ or $UCl_{4(g)}$. With Uranium tetrachloride (UCl_4), boiling point of 1064K and Uranium hexafluoride (UF_6), boiling point of 330K, collection of crud at the collection reservoirs is a problem, but with $Kr_{(g)}$ this problem will not be an issue.

Many isotope separation techniques, such as laser techniques, chemical reaction rate techniques, liquid thermal diffusion, gravity or cryogenic distillation and many others are available, but will not be described here.

3.2.4 Theory of Present Experiment

Dr. Mills and Dr. Bader have simulated a system of Krypton isotopes desorbing from a graphite surface and found that multilayer system behaves in accordance with

Graham's Law, but a monolayer of adsorbed Krypton isotopes desorbs at a much higher rate. Presented work is built on that research[9].

Adsorption is defined as the adhesion of atoms or molecules to a surface. Exact details responsible for adsorbance to the substrate are highly specific to the atomic or molecular species, but generally main forces responsible are Van Der Waal forces, especially in the case of rare gas isotopes for which the polarizability is very small. Desorption is the opposite of adsorption and is defined as a substance being released from or through a surface. The rate of desorption (R), may be described by the following equation:

$$R = kN^x$$

Where k is the rate constant and N is the surface concentration of the species that is adsorbed onto the surface. Desorption order (x) can usually be predicted[9] in accordance with the type:

Atomic desorption: first order process (x = 1)

$$Kr_{(adsorbed)} \rightarrow Kr_{(gas)}$$

Recombinative Process: second order process (x = 2)

$$2O_{(adsorbed)} \rightarrow O_{2(gas)}$$

The rate constant (k) could be expressed with Arrhenius equation [10] form where A is the pre-exponential factor describing the attempt frequency of the atom or molecule to overcome the barrier to desorption [11]. The exponential term ($e^{-\frac{E_a}{RT}}$) gives the fraction of atoms which have the energy equal to or greater than the activation energy. General

assumption is that both the attempt frequency and desorption energy are dependent on temperature and coverage [9].

$$k = AN^{-1}e^{-\frac{E_a}{RT}}$$

In combination of the two, desorption rate (R) can be expressed as a function of temperature.

$$R = AN^{-1}e^{-\frac{E_a}{RT}}$$

In the simulation, Dr. Bader and Dr. Mills have kept temperature constant, at 120K, in order to study the system with a reasonable number of time steps. With the simulation, a 5-layer system was in agreement with Graham's Law and the ratio of desorbed light

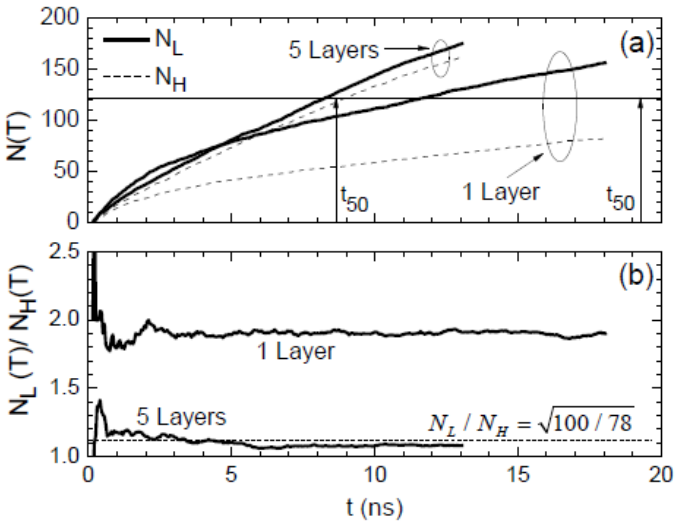

Figure 3.6 (a) Number of light (N_L, Kr_{78}) and heavy (N_H, Kr_{100}) isotopes that have desorbed from the surface as a function of time for 1 and 5 adsorbed layers at 120K.
(b) Ratio of desorbed isotopes N_L/N_H vs. time.
Reproduced image from reference [4]

isotopes in comparison to heavy isotopes ($\frac{Kr_{78}}{Kr_{100}}$) stabilized at $\sqrt{\frac{100}{78}} = 1.13$ as one would expect. However, a monolayer system exhibited a ratio of 1.9, which is significantly higher. The reproduced image from Dr. Bader's dissertation clearly shows the difference in desorbance between the number of light isotopes (N_L) and the number of the heavy ones (N_H). For the monolayer system, the fact that lighter isotopes are desorbing at a higher rate than the rate predicted by the Graham's Law, means that this could be the basis for a more efficient way to separate isotopes.

Higher efficiency of Krypton isotope separation per stage utilizing monolayer method, would cut down on the number of stages needed to achieve the desired isotope purity, compared to the gas diffusion or centrifuge methods that operate at Graham's Law separation ratios. As a bonus, with the reduced number of moving parts, it would mean that in comparison with centrifuge facility, monolayer separation facility would need lower number of man-hours to maintain it. The robustness of the equipment would be much higher and therefore increased safety for staff.

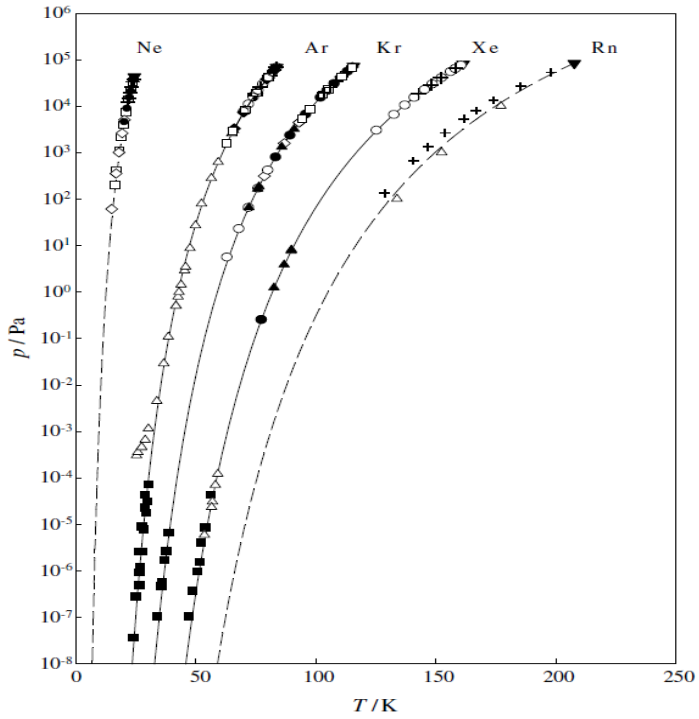

Figure 3.7 Sublimation curves of the rare gases**.** Reproduced from reference [7]

3.3 Experimental set up for $Kr_{(g)}$ monolayer separation investigation

For the proposed experiment of Krypton isotope separation through the monolayer sublimation process, a temperature range of 40-55K was selected. Such temperatures are in the range needed to keep the Kr gas pressure in the range between 10^{-9} to 10^{-7} torr as Krypton gas is introduced and frozen inside the chamber. Figure 3.7 used to estimate expected freezing and sublimation temperatures for the Krypton gas[12]. These low pressures were required since the Residual Gas Analyzer (RGA) can only be

run at pressures lower than 10^{-5} Torr, in order to avoid damages to the electron multiplier and possibly other components during operation.

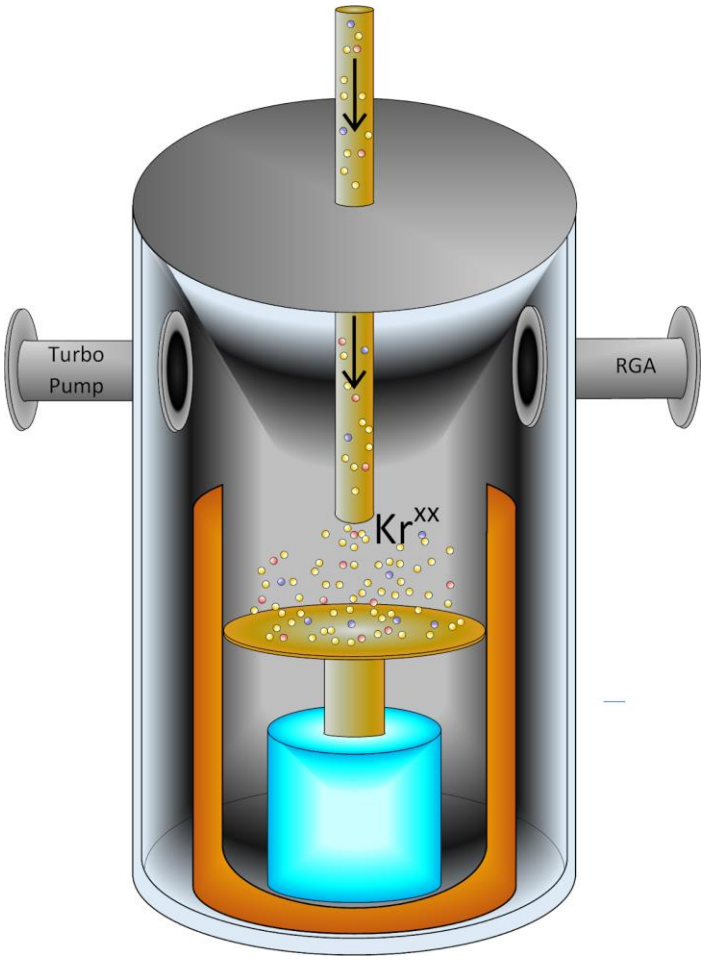

Figure 3.8. Cu ¼ inch tube feeds $Kr_{(g)}$ onto ~5cm diameter Cu substrate, which is cooled by the Cold-head behind the Cold-head heat shield. Heating element is mounted underneath the Cu substrate.

Figure 3.8 shows the set up used to collect data. The cold finger was hidden from the outside chamber by the heat shield in order to get to low temperatures required.

Copper substrate was machined to fit inside the heatshield and attach to the cold finger via ¼-28 hex screw with a spring washer present. Spring washer was included in order to mitigate possible problems due to negative thermal expansion of the metals during temperature changes between 30K and room temperature. For copper (99.99% purity) thermal expansion coefficient (α) is $2.278\times10^{-6}\,\frac{m}{m^{\circ}C}$ (at 40K)[13] and using the thermal expansion equation change in length (ΔL) could be calculated as follows:

$$\Delta L = \alpha L \Delta T = 2.278 \times 10^{-6}\left(\frac{m}{mK}\right) \times 0.040m \times (293.15 - 40.0)(K) = 2.3 \times 10^{-5}m$$

For a 4 cm copper rod connecting the copper substrate to the cold head, a 23 μm contraction could theoretically occur. Hex screw's stainless-steel thermal expansion coefficient is different, therefore change in length for the hex screw will not the same as copper parts. Such changes in lengths of metal components could affect the integrity of the connection between cold finger and the substrate, onto which Krypton gas is deposited on. The spring washer is therefore included in the design to mitigate the possibility of disruptions in continuous heat flow to the system and avoid possible experimental error. Figure 3.9 illustrates the set up.

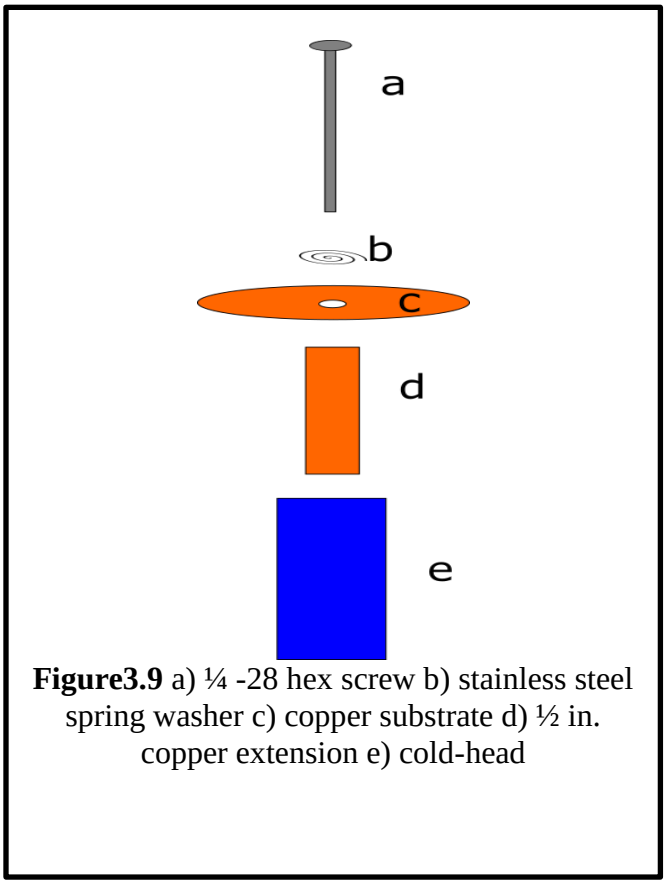

Figure3.9 a) ¼ -28 hex screw b) stainless steel spring washer c) copper substrate d) ½ in. copper extension e) cold-head

Heating element was installed to the bottom of the copper substrate plate. A separate power supply was feeding the current through the heating element with high precision (±0.01A) in order to control the heating rate of the substrate. Copper is among the highest heat conducting materials, so there was no issue of heating the whole substrate with the small radius of 3.5 cm with a single heating element. Cylindrical heating element was, additionally, pressed against a thin sheet of indium to increase the interface surface area between the body of the heating element and the substrate. Indium is a soft metal, so with minimal pressure it ensures a good contact by forming around the

curved cylindrical body of the heating element and the flat surface of the copper substrate.

Heat shield outside of the cold head minimizes the ingress of the environmental heat coming from the room temperature steel body of the vacuum chamber. The amount of heat that the cold head can pump out would be overwhelmed by the amount of heat coming in from the inside of the chamber walls and stabilize around 80K or above. As discussed above, these temperatures are too high for the Krypton gas to be frozen onto the surface of the substrate. The heat shield is made of a reflective insulating material in order to prevent as many methods of heat conduction as possible, such as black body radiation, conduction and convection. With this concept in mind, the substrate had to be hidden behind the heat shield.

Microleak valve is the means of introduction of Krypton gas into the chamber. A quarter inch diameter copper tube was connected to the microleak valve output inside the chamber, and the end of the tube is 2.5 cm above the cold head substrate. The copper tube serves as means of delivering Krypton gas closer to the substrate, instead of just filling the chamber up with the gas. The copper tube opening 2.5cm from the cold finger allowed for more even dispersion of Krypton gas onto the substrate surface.

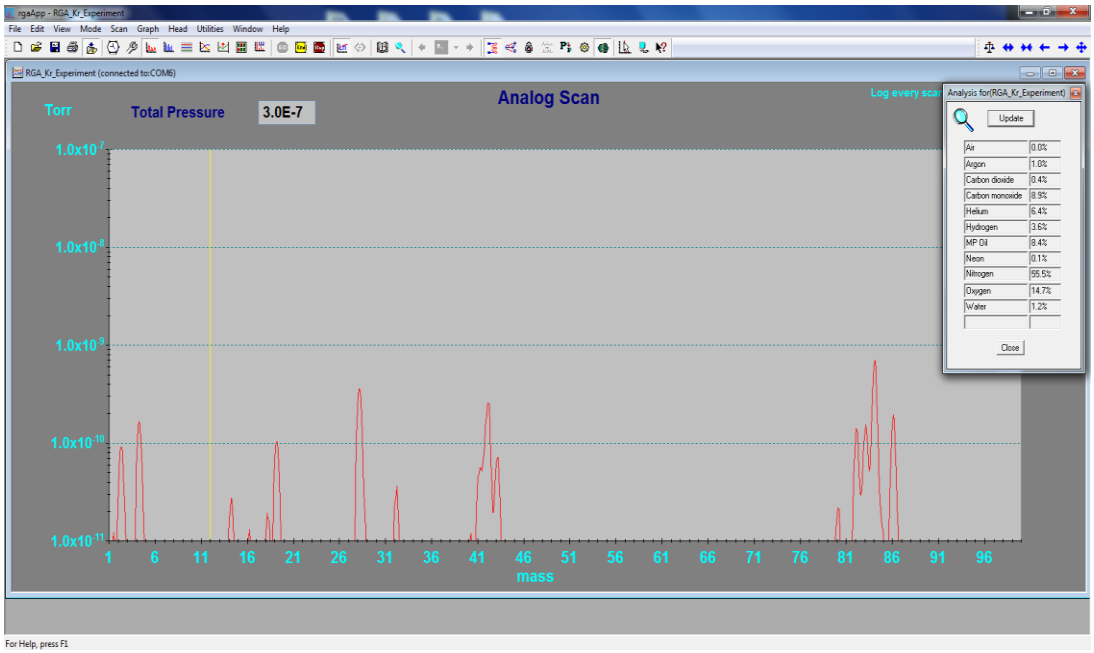

Figure 3.10 Gas make up scan inside the chamber before turning on the cold head

A Pfeifer pressure gauge Model PKR 251 was installed onto the chamber in order to track pressure ranges inside the chamber in the beginning of the pump down of 760 Torr, down to 10^{-5} Torr. Once pressures below 10^{-5} were reached a residual gas analyzer was turned on to accurately track the pressures and gas compositions inside the chamber as shown in Figure 3.10. The chamber was baked over night at a moderate temperature of 70 ℃ to expel as much water vapors and other volatile components as possible. Water vapors freezing onto the cold surface of the substrate could be introducing variability to the results and be a cause of systematic error. A sudden pressure drop inside chamber, when the cold head was turned on, was a sign of gases freezing onto the cold surfaces. With starting pressures of 10^{-7} Torr prior to turning on of the cold head, the amount of gas frozen onto the surfaces of the cold head was minimized. The final iteration of the set

up was capable of 40K substrate temperature and base pressure ranges between 10^{-9}-10^{-8} Torr.

Once the necessary temperature (40-48K) and pressure (10^{-9}-10^{-8} Torr) ranges were reached, the experiment could begin. Krypton gas was introduced into the chamber via the microleak valve. Number of opening turns and time in open position were optimized based on the collected data from the RGA. The RGA was set for tracking the six Krypton isotope partial pressures. The user interface (UI) was built using the LabVIEW software in order to collect and record data. Native software was used for the data collection and recording from the RGA apparatus. Figure 3.11 is an example of the UI at the conclusion of the run.

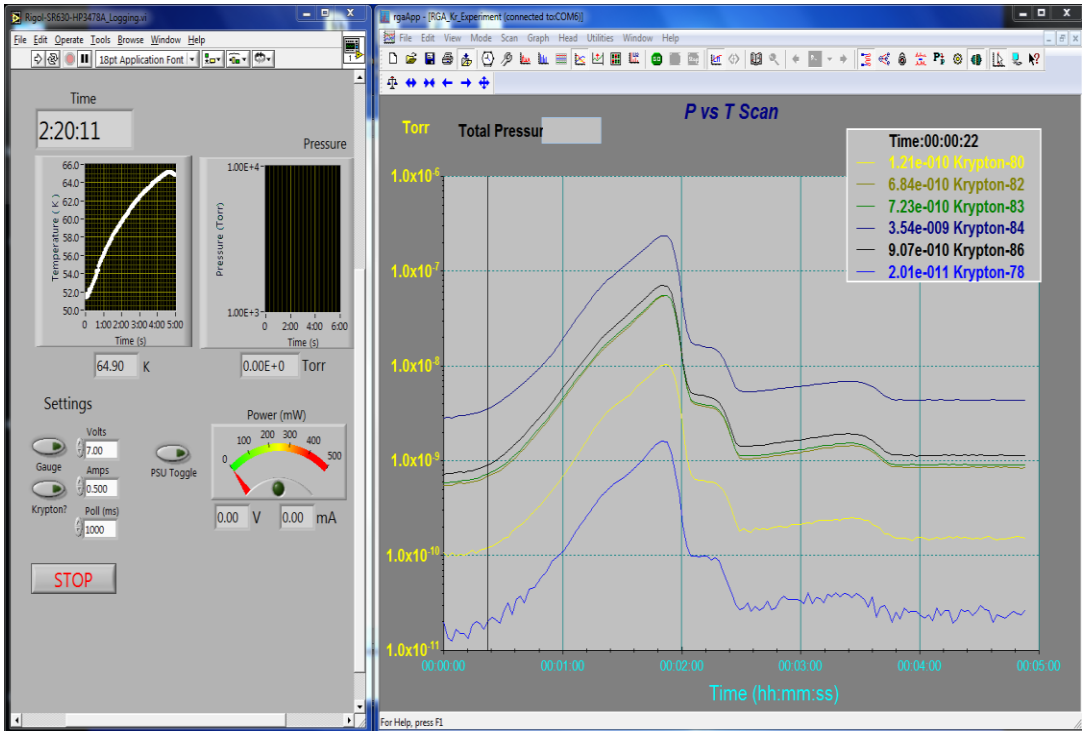

Figure 3.11 User Interface (UI) and sample recorded partial pressure scan for the tracking of Krypton isotope pressures during desorption

3.4 Experimental results

Simulations by Bader suggest that when there are only a few monolayers of gas present on a surface, the different mass isotopes should desorb at rates proportional to the isotopic mass raised to a power greater than the -½ power predicted by Graham's Law. Experimentally we expect to see a pressure increase of lighter isotopes to be higher than that of heavier isotopes. Due to the small amount of gas frozen onto the substrate, the pressure gauges have to be very sensitive. The RGA's accuracy rated to 10^{-11} Torr makes it the most reliable measuring device available for the experiment.

From the collected data, a few interesting results were seen. Figure 3.15 show the normalized partial isotopic pressures during the experiment. As expected, during the heating phase, the pressures began to rise and peaked around 57±5K. After each run, the substrate was heated up to 65K to ensure full Krypton gas desorption before the next run. The main bump in figure 3.13 is behaving as expected, with rising temperature, so did the pressure. The interesting part of the figure 3.13 is at the end, when the pressure starts to drop after the 2-minute mark, while the temperature is still rising at constant rate, this signifies that the substrate is running out of the Krypton ice. With constant evaporation rate to go on as it has, we'd expect to see a smooth pressure drop, but we see a final bump in pressure. This could be significant in case we are witnessing a sudden rise in the rate of sublimation for the last monolayer of the Krypton ice. Also, it would be similar with Dr. Bader's evaporation rate being different between bulk and monolayer systems of Krypton ice. Figures 3.12 and 3.13 show consistent presence of this evaporation rate effect.

In order to rule out the possibility of uneven heating of the copper substrate, we calculated that with 1-watt energy input from the heating element into the copper substrate, there would be approximately a difference of 0.01K from the opposite edges separated by 5cm diameter. This would be a negligible temperature difference and wouldn't explain the difference in sublimation rates.

Figure 3.15 shows the difference in relative abundances as a function of time and figure 3.12 is the pressure data for the experimental run. This way it possible to visualize the changes in presence of each isotope as a function of time. There seems to be a trend for isotopes Kr-80, Kr-82, Kr-83, Kr-86 to increase, while the Kr-78 and Kr-84 are on the decrease. Kr-78 had the lowest pressures due to general accepted relative abundance of this isotope being the lowest, which was consistent with collected data. However, Kr-78 pressures were near the detection limit of the RGA with the pressures oscillating in the 10^{-11} Torr. With background signal of comparable size, data collected for Kr-78 was very noisy. This leaves room for future experimental improvements. With 3.14 graph, we saw that most stable (Kr-84) isotope's abundance was dropping, while the lower abundance isotopes (Kr-80, Kr-82 and Kr-83) had a positive slope at around 81 seconds mark.

3.5 Conclusion

In conclusion, looking at data is from Run 0 and Run 2, while there is no convincing evidence of a dependence of the rate of evaporation on the isotope mass, there is an obvious increase in the vapor pressure in the last stages of the evaporation of a film.

From the sharp drop in pressure around 300 s one may estimate the Kr is evaporating at a rate of about 1 ml per 10 sec. This effect may arise from the roughness of the Kr associated with the diffusion of the gas molecules providing increasingly opportune geometries with low surface binding energies as the layer gets thinner and thinner.

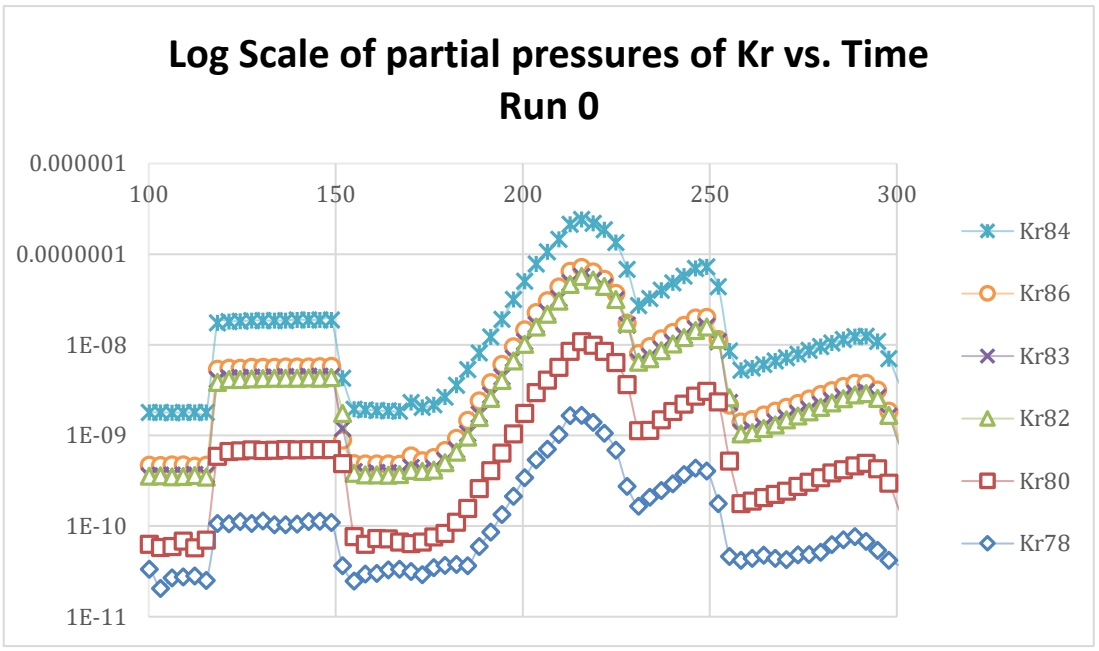

Figure 3.12 Log scale of partial pressures for Krypton isotopes vs time for run #0.

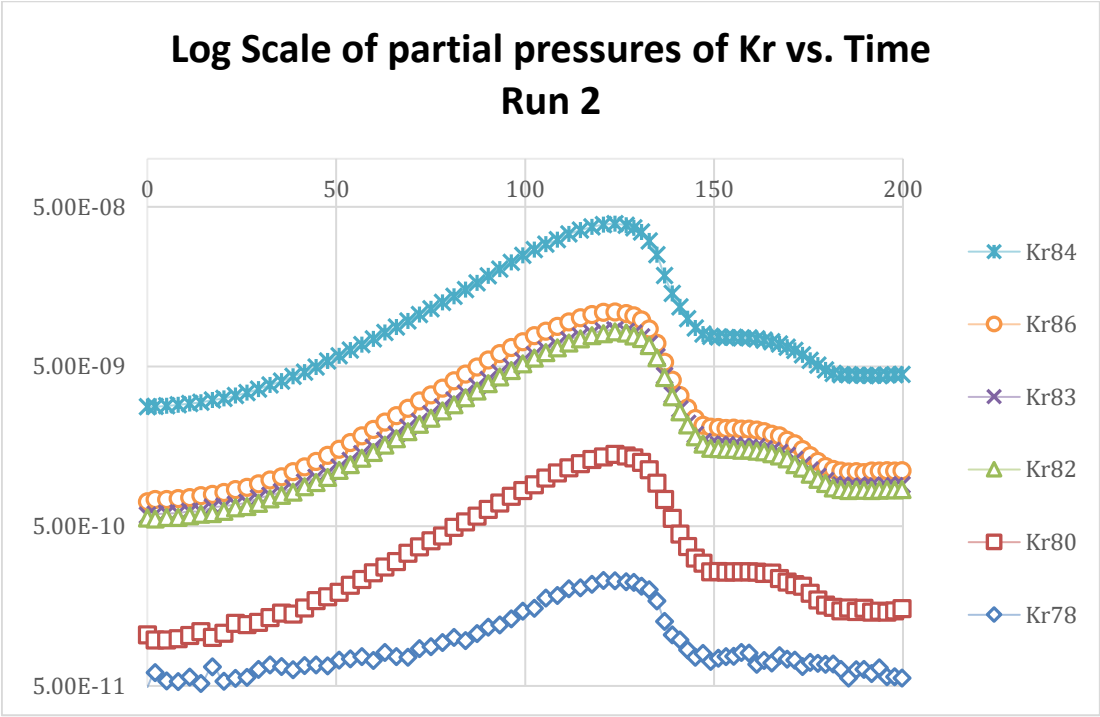

Figure 3.13 Log scale of partial pressures for Krypton isotopes vs time for run #2.

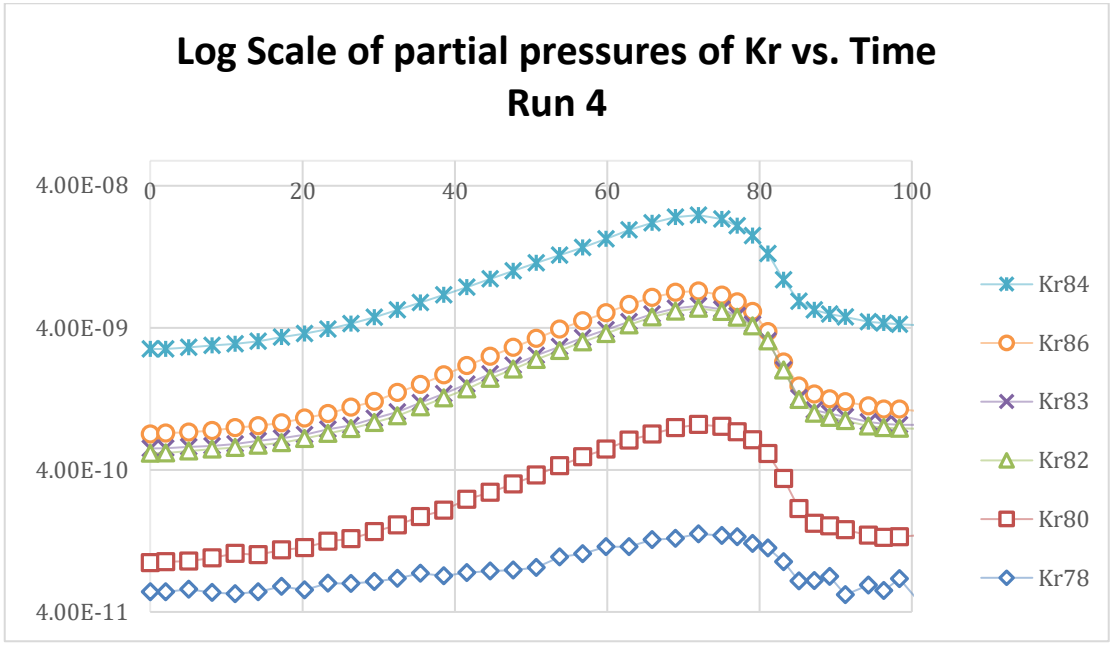

Figure 3.14 Log scale of partial pressures for Krypton isotopes vs time for run #4.

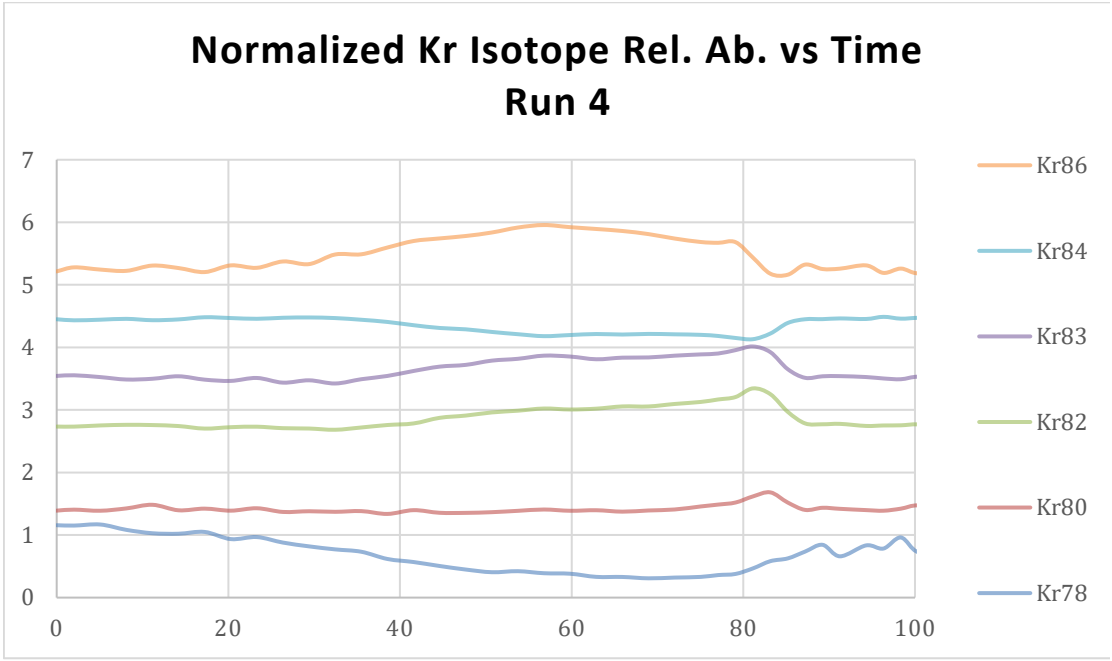

Figure 3.15 Relative abundance curves for each isotope calculated for each time step of the experiment and normalized.

3.6 References

[1] F. W. Soddy, “Intra-atomic Charge,” *Nature*, no. 92, pp. 399–400, 1913.

[2] G. B. Kauffman, R. D. Ebner, G. B. Kauffman, and R. D. Ebner, “Gaseous Difíusion : A Demonstration of Graham ’ s Law,” vol. 15, no. 1, pp. 78–79, 2020.

[3] W. D. . Harkins, “The Separation of the Element Chlorine into Chlorine and Meta-Chlorine,” *Science (80-.).*, vol. 51, no. 1316, pp. 289–291, 1920.

[4] W. D. H. and T. H. Liggett, “Separation of the Chlorine isotopes,” *J Phys Chem*, vol. 28, no. 74, 1924.

[5] K. C. and G. Dickel, *Zur Trennung der Chlorisotope, Die Naturwissenschaften*. 1939.

[6] J. W. Beams and F. B. Haynes, “The separation of isotopes by centrifuging,” *Phys. Rev.*, vol. 50, no. 5, pp. 491–492, 1936, doi: 10.1103/PhysRev.50.491.

[7] “Electromagnetic Separation (Calutron) and Thermal Diffusion.” 2008, [Online]. Available: https://www.nrc.gov/docs/ML1204/ML12045A056.pdf.

[8] D. R. Smith, “The Calutron Girls.” http://exploreoakridge.com/who-were-the-calutron-girls-of-oak-ridge/.

[9] K. D. W. Bader, “Molecular Dynamics Study of Isotope Separation via Physisorbed Systems,” *Dissertation*, no. June. 2012.

[10] Laidler, K. J. (1987) *Chemical Kinetics*, Third Edition, Harper & Row, p. 42.

[11] H. A. and M. Masuda, “Bilayer Modelfor Zero Order Desrption,” *Surf. Sci.*, vol. 207, pp. 517–524, 1989.

[12] A. G. M. Ferreira and L. Q. Lobo, “The sublimation of argon, krypton, and xenon,” *J. Chem. Thermodyn.*, vol. 40, no. 12, pp. 1621–1626, 2008.

[13] F. R. Kroeger and C. A. Swenson, “Absolute linear thermal-expansion measurements on copper and aluminum from 5 to 320 K,” *J. Appl. Phys.*, vol. 48, no. 3, pp. 853–864, 1977, doi: 10.1063/1.323746.